

# Selection and Validation of Charge and Lennard-Jones Parameters for QM/MM Simulations of Hydrocarbon Interactions with Zeolites

Paul M. Zimmerman,<sup>†</sup> Martin Head-Gordon,<sup>\*,†</sup> and Alexis T. Bell<sup>‡</sup>

<sup>†</sup>Department of Chemistry, University of California, Berkeley, California 94720-1461, United States

<sup>‡</sup>Department of Chemical and Biomolecular Engineering, University of California, Berkeley, California 94720-1462, United States

**ABSTRACT:** Quantum mechanics/molecular mechanics (QM/MM) models are an appealing method for performing zeolite simulations. In QM/MM, a small cluster chosen to encompass the active center is described by QM, while the rest of the zeolite is described by MM. In the present study, we demonstrate that the charges and Lennard-Jones parameters on Si and O must be chosen properly for QM/MM calculations of adsorption energies and activation energies to agree closely with full QM calculations. The selection of parameters for Si and O is based on using the  $\omega$ B97X-D functional for DFT calculations of the QM region, which is effective in capturing the effects of van der Waals interactions. A comparison of the heats of adsorption for a variety of adsorbates and activation energies for the cracking of propane and butane reveals that energies derived from QM/MM calculation carried out with appropriately selected MM parameters agree to within an rms error of  $\sim 1.5$  kcal/mol with QM calculations. To avoid reparametrization for new substrates, Lennard-Jones zeolite parameters are chosen to be compatible with existing CHARMM parameters. Transferability of these parameters is demonstrated by tests utilizing the B3LYP density functional and simulations of MFI and FAU zeolites. Moreover, the computational time for QM/MM calculations is considerably lower than that for QM calculations, and the ratio of computational times decreases rapidly with increasing size of the cluster used to represent the zeolite.

## INTRODUCTION

Zeolites are crystalline microporous solids composed of corner-sharing, tetrahedrally coordinated silicate ( $\text{SiO}_4$ ) units. Isomorphic substitution of Si atoms by Al atoms and a charge-compensating proton ( $\text{HAlO}_4$ ) introduces Brønsted acidic bridge-bonded hydroxyl groups. Zeolites in this form are solid acids widely used to catalyze a variety of reactions, e.g., cracking, isomerization, and alkylation, involved in the conversion of petroleum to transportation fuels and the production of commodity and specialty chemicals.<sup>1–4</sup> Substitution of the Brønsted-acid protons by metal cations enables zeolites to serve as catalysts for other reactions, such as the selective reduction of NO, the decomposition of  $\text{N}_2\text{O}$ , oxidation of olefins, the carbonylation of alcohols, etc.<sup>5</sup> In these reactions, the metal cation acts as either a Lewis acid or a redox center. Experimental studies have shown that the activity and selectivity of both Brønsted-acid and metal-containing zeolites are strong functions of their architecture and Si/Al ratio.<sup>4</sup> Since the number of possible zeolite structures exceeds those used commercially by several orders of magnitude,<sup>6–10</sup> it would be highly desirable to predict how zeolite structure and composition affect the activity and selectivity of zeolite catalysts. An attractive approach to this end is the use of quantum chemical calculations to describe the electronic and catalytic properties of catalytically active sites located within the pores and channels of zeolites. Molecular-scale information that is often difficult, and sometimes not possible, to obtain otherwise can be obtained by this means.<sup>11,12</sup> Examples include the geometry, energy, and vibrational spectrum of ground and transition states, and the dynamics of elementary processes involved in the transformation of reactants to products. Such calculations are also useful for confirming interpretations of adsorbate structure and reaction mechanisms

deduced from experimental evidence and for assessing the impact of zeolite architecture and composition on catalyst activity and selectivity.

The application of quantum mechanics to chemical reactions occurring in zeolites is particularly challenging because of the large number of atoms required to capture the long-range Coulombic and van der Waals interactions. Ab initio wave function theories (MP2, CCSD(T), etc.) cannot be carried out for such systems because they scale with the fifth power or more of the number of atoms in the system. Consequently, most investigations of reactions occurring in zeolites are based on density functional theory<sup>13</sup> (DFT), which scales with no worse than the third order of the number of atoms. While the computational cost of DFT calculations is acceptable for many applications, the accuracy of the method depends on the exchange-correlation functional. Recent work has demonstrated that the popular B3LYP functional<sup>14</sup> does not capture the effects of dispersive interactions adequately, leading to significantly inaccurate heats of adsorption and activation energies.<sup>15,16</sup> Of the various functionals developed over the last several years, the two that have been demonstrated to be most effective in capturing van der Waals interactions in zeolites are MO6-2X<sup>17</sup> and  $\omega$ B97X-D.<sup>18</sup>

Recent studies utilizing density functional theory (DFT) have shown that in order to achieve results consistent with experimental results, it is necessary to use large cluster representations of the active center and surrounding portion of the zeolite framework as well as a functional that properly accounts for dispersion. Although DFT is much more efficient computationally relative to other

Received: March 9, 2011

Published: May 20, 2011

**Table 1. Sampling of Charges Used for Si in QM/MM Simulations of Zeolites in the Literature**

Si charge (au)	explanation	reference
0.0	mechanical embedding	48
1.0	Mulliken from DFT	39
1.2	potential derived charge from DFT	49
1.2	taken from MM parameter set	50
1.84	fit to Hartree–Fock	51
2.0	one-half of formal charge	26, 52
4.0	formal charge	53

electronic structure theories, its  $\sim N^3$  scaling means that computations with the large clusters required to capture the effects of dispersive and electrostatic interactions are prohibitively slow. For this reason, it is very difficult to achieve convergence of calculated thermochemical properties to values observed experimentally with increasing cluster size.<sup>19</sup> To overcome the electrostatic issue, some researchers have utilized periodic boundary conditions to represent the extended framework.<sup>20,21</sup> However, these simulations remain computationally intractable for large zeolite unit cells. Periodic simulations of the active site and associated molecules can result in the experience of dipole–dipole interactions with periodic images, which may influence the quality of the results. An additional limitation of periodic boundary simulations is that the algorithms used for such calculations cannot readily utilize advanced functionals, such as  $\omega$ B97X-D, due to difficulties in computing exact exchange.

Several authors have explored the option of carrying out hybrid quantum mechanical/molecular mechanical (QM/MM) simulations as a means for balancing accuracy and computational time for very large systems.<sup>22–27</sup> In this formalism, reactive atoms (the active site and reagents) are represented by DFT (or other *ab initio* method), and nonreacting atoms are represented by a molecular mechanics (MM) force field. This division is natural in zeolites and allows for bond-breaking to be described in the QM region and other important, but more distant, interactions to be captured by interactions with the MM region. QM/MM is vastly more computationally efficient than QM and therefore well suited for investigating large zeolite frameworks.<sup>24–30</sup> However, it must be recognized that the accuracy of QM/MM simulations depends critically on the functional used for the DFT calculations and also the choice of charges and Lennard-Jones parameters used for the MM calculations. Surprisingly, this issue has not been investigated in a systematic manner. As may be seen from Table 1, a wide range of charge parameters have been used by different authors. In some cases, formal charges have been used, while in other cases charges were adjusted to replicate the results of Hartree–Fock calculations. It should also be noted that, in some simulations, MM–QM electrostatics have been neglected, even though this mechanical embedding poorly represents the polarized Si–O bonding.

In this paper, we describe the selection and validation of MM parameters tailored for zeolite QM/MM simulations. Using the parameters determined in this study, QM/MM is shown to reproduce accurately QM geometries and QM energetics to within  $\sim 2$  kcal/mol. Furthermore, these parameters work well with both  $\omega$ B97X-D and B3LYP functionals. In our QM/MM implementation, we employ static point charges in an electrostatically embedded model with Lennard-Jones potentials to

account for dispersion interactions. The Lennard-Jones parameters are chosen such that the adsorbate Lennard-Jones parameters can be taken directly from the existing CHARMM parameters. Because this is a simple electrostatic embedding model with a standard form of empirical dispersion, we anticipate that the parameter set will be highly useful for existing QM/MM implementations.

## COMPUTATIONAL METHODS

**Zeolite Geometries.** The crystallographic structures of MFI<sup>31</sup> and FAU<sup>32</sup> were used to determine the positions of all atoms in the zeolites. Although Al can be located in 12 symmetrically distinct positions in MFI, different in energy by only a small amount, there is evidence that the T12 position is favored.<sup>33,34</sup> Therefore, the T12 site was chosen for the calculations reported here. Zeolite clusters with 23 and 44 tetrahedral atoms (T23 and T44) were generated for MFI. Calculations were done for FAU using a T52 cluster. Since all T sites have the same symmetry in FAU, the placement of the Al atom is not critical for FAU. Each of the clusters was terminated with hydrogen atoms positioned on the vector between the terminal Si atoms and the replaced O atoms, located 1.47 Å away from the terminal Si atoms. During geometry optimizations, the lattice atoms away from the T5 region were kept frozen at their crystallographic positions.

**QM Computations.** Calculations were performed with DFT/ $\omega$ B97X-D in order to provide benchmarks for verifying the results of QM/MM. Geometries were optimized using the  $\omega$ B97X-D functional and the double- $\zeta$ , polarized 6-31G\* basis set, and single point DFT energies were then determined with the augmented, polarized 6-31+G\*\* basis set. Geometries were reoptimized with B3LYP and 6-31G\* for the B3LYP test set. All QM computations were performed using Q-Chem.<sup>35</sup>

**QM/MM Setup.** Multiple strategies exist for implementing QM/MM simulations,<sup>22–27</sup> all of which begin by dividing the atoms of the system into QM and MM regions. Notable for zeolite simulations are Sauer's QM/shell model<sup>28,29</sup> and Morokuma's ONIOM method.<sup>30</sup> These two approaches involve mechanical embedding of the QM region and can include empirical dispersion interactions between the regions. Since MM–QM electrostatic interactions are not considered, polarization of the active site by the lattice is, therefore, excluded. Our QM/MM implementation follows the method of ref 36, where both dispersion and electrostatics are treated between the QM and MM regions (i.e., electrostatic embedding<sup>22</sup>).

The division between QM and MM regions is described in Figure 1. To divide the QM and MM regions smoothly, a single hydrogen link atom is used to replace a Si–O bond at the terminus of the QM cluster.<sup>37</sup> The terminating H atoms were placed along each of the terminal Si–O bonds at a distance of 0.92 R(Si–O) from the terminal Si atom. Typical Si–H link atom bond lengths were approximately 1.47 Å. To achieve charge neutrality of the MM subsystem, a fraction of the link atom charge was added to its covalently bonded neighbor, and the charge on the link atom was set to zero. Failure to neutralize the MM region caused significant errors in the absorption energies of polar species; therefore, neutrality of the MM region was maintained for all simulations. Except where noted, the QM region was a T5 cluster centered on the zeolite acid site. While other strategies have been used for QM/MM simulations,<sup>38,39</sup> these approaches are more complicated and require additional parametrization.

The MM region was described by a standard force field of the CHARMM type.<sup>40</sup> The most important terms in the force field are the electrostatic energy,

$$E_{\text{ES}} = \sum_{ij} \frac{q_i q_j}{4\pi\epsilon_0 r_{ij}} \quad (1)$$

and the Lennard-Jones potential energy

$$E_{\text{LJ}} = \sum_{ij} \epsilon_{ij} \left[ \left( \frac{R_{ij}}{r_{ij}} \right)^{12} - 2 \left( \frac{R_{ij}}{r_{ij}} \right)^6 \right] \quad (2)$$

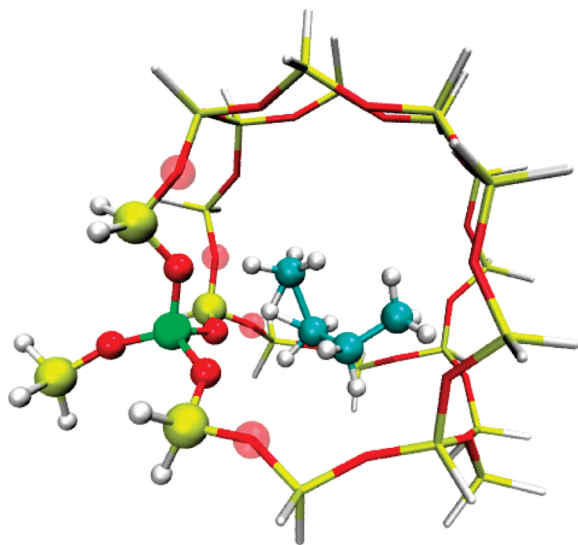


**Figure 1.** Schematic of the division between QM and MM regions. Spherical atoms are QM, and transparent atoms are link atoms. The QM region is polarized by atomic partial charges in the MM region. The immediate Si neighbors to the link atoms are assigned a smaller charge to create an overall neutral MM region. Lennard-Jones potentials are applied to pairs of atoms that include at least one MM atom to account for dispersion.

where  $\epsilon_{ij} = (\epsilon_i \epsilon_j)^{1/2}$  and  $R_{ij} = (R_i + R_j)/2$ . These expressions require three parameters for each atom type:  $q_i$ , the atomic partial charge;  $R_i$ , the van der Waals radius; and  $\epsilon_i$ , the characteristic energy for the Lennard-Jones potential. A point charge model was used instead of more sophisticated polarizable models to allow compatibility with existing electrostatically embedded QM/MM implementations. While simple, this approach yielded results of sufficiently high accuracy. To avoid modifying parameters of nonzeolite molecules, CHARMM parameters were utilized for the atoms of the molecules interacting with the zeolite. QM/MM simulations were performed utilizing a development version of the Q-Chem software package.<sup>35</sup>

## PARAMETER SELECTION

Because most of the atoms in the zeolite lattice were kept frozen at their crystallographic positions, we focused on determining reliable atomic charges and Lennard-Jones parameters for Si and O, while the MM bonding parameters remain unchanged. Since our approach selects MM parameters specifically for QM/MM use, we used the CHARMM parameters for silica<sup>41</sup> as a reasonable starting point. This set of parameters (referred to below as parameter set P1) was developed using the standard CHARMM procedure that ensures consistency with existing CHARMM parameter sets.<sup>40</sup> While the parameters for Si and O determined by this means are suitable for CHARMM MM simulations, they are not necessarily reliable for use in QM/MM simulations.

Selection of a satisfactory set of charge and Lennard-Jones parameters for Si and O was done by reducing the error between QM/MM and QM calculations carried out for three test sets. For each one, the van der Waals radii,  $R_i$ , for Si and O in CHARMM were maintained, and only the energy parameters,  $\epsilon_i$ , were adjusted along with the charge parameters. The first test set examines the adsorption of methane, ethane, propane, and butane in purely siliceous MFI (silicalite), represented by a T23 cluster. For this set of molecules, adsorbate–zeolite interactions are dominated by dispersive forces. The second test set examines the interactions of propane, CO, acetonitrile,  $\text{NH}_3$ , and

**Table 2.** Quantum Mechanical Absorption Energies and Apparent Activation Energies from  $\omega$ B97X-D and Experiments (kcal/mol)

		B3LYP	$\omega$ B97X-D	$\omega$ B97X-D	exp. $\Delta H_{\text{abs}}$	ref.
		6-31G*	6-31G*	6-31+G**		
T23 MFI (all silica)	methane	1.3	−4.2	−3.8	−4.8	54
	ethane	−0.7	−7.7	−7.8	−7.9	54
	propane	−0.4	−10.9	−9.3	−9.6	54
	butane	−2.6	−14.7	−13.9	−11.7	54
T44 H-MFI	propane	−0.4	−12.2	−13.7	−11.0	55
	CO	−7.4	−10.8	−10.2	−6.3, −8.0	56, 57
	acetonitrile	−16.8	−25.8	−24.7	−26.3	58
	$\text{NH}_3$	−28.3	−33.6	−30.0	−34.7	59
	pyridine	−27.2	−42.9	−46.8	−47.6	59
		6-31G*	6-31G*	6-31+G**	exp. apparent $\Delta H^\ddagger$	
T23 H-MFI	propane cracking	45.2	32.0	30.7	37.0, 35.1	60, 61
	propane H-exchange	28.3	22.8	20.3	n/a	
	butane cracking 1	42.2	26.8	26.2	32.3	60
	butane cracking 2	42.1	26.2	25.3	32.3	60



pyridine with a Brønsted acid site in H-MFI, represented by a T44 cluster. This group contains larger molecules that are more sensitive to long-range charge interactions with the lattice and molecules such as  $\text{NH}_3$  and pyridine that can interact strongly with the Brønsted acid proton of the zeolite. The third test set examines the activation barriers for hydrogen exchange and cracking of propane, and for *n*-butane cracking at the C1 and C2 positions. A T23 H-MFI cluster was used for these calculations.

The accuracy of the QM calculations was established by comparison with experimental values. As seen in Table 2, the QM calculations carried out at the  $\omega\text{B97X-D}/6\text{-}31\text{G}^*$  and  $\omega\text{B97X-D}/6\text{-}31+\text{G}^{**}$  levels for the first test set agree closely with the experimental values of the heats of adsorption for methane, ethane, propane, and butane. However, similar calculations carried out with B3LYP/6-31G\* yield heats of adsorption that are consistently lower than those calculated with  $\omega\text{B97X-D}/6\text{-}31\text{G}^*$  and those observed experimentally, confirming the superior performance of the  $\omega\text{B97X-D}$  functional for describing dispersive interactions. Similar conclusions can be drawn by examining the results for a second test set. It is also noted that the strong interactions of pyridine, acetonitrile, and ammonia with the Brønsted acid site are well described using the  $\omega\text{B97X-D}$  functional. For the third test set, QM calculations carried out at the  $\omega\text{B97X-D}/6\text{-}31\text{G}^*$  and  $\omega\text{B97X-D}/6\text{-}31+\text{G}^{**}$  levels underpredict the experimentally observed apparent activation barriers by about 5–6 kcal/mol (i.e., the energy difference between the transition state and the molecule in the gas phase), but are consistently better than calculations done at the B3LYP/6-31G\* level, which tend to overpredict activation barriers by about 10 kcal/mol.

Because the  $\omega\text{B97X-D}$  functional produced results in good agreement with experimental ones, QM/MM parameters were selected to reproduce these QM results. Figure 2 outlines a general methodology for generating reliable charge and L-J parameters for zeolites. After comparing the results from QM to QM/MM with the CHARMM parameter set (P1), the L-J parameters are modified. QM/MM computations are repeated holding the charge constant until a small value of rms error is

achieved. This procedure produces the P2 parameter set. Having determined the L-J parameters, these are fixed and a similar iterative procedure evaluates the charge parameters. The lowest rms errors resulted from parameter sets P3 and P4. Finally, a mechanically embedded parameter set, P5, is constructed by setting the charge to zero.

These sets, presented in Table 3, are P1, the CHARMM set of charges and Lennard-Jones parameters for Si and O determined for silica ( $Q_{\text{Si}} = 1.08$ ,  $Q_{\text{O}} = -0.54$ ,  $\epsilon_{\text{Si}} = 0.6$  kcal/mol, and  $\epsilon_{\text{O}} = 0.1521$  kcal/mol); P2, the CHARMM charges for Si and O and the new set of Lennard-Jones parameters found in this work ( $Q_{\text{Si}} = 1.08$ ,  $Q_{\text{O}} = -0.54$ ,  $\epsilon_{\text{Si}} = 0.2$  kcal/mol, and  $\epsilon_{\text{O}} = 0.075$  kcal/mol); P3, the first set of reduced charges on Si and O and the new set of Lennard-Jones parameters ( $Q_{\text{Si}} = 0.80$ ,  $Q_{\text{O}} = -0.40$ ,  $\epsilon_{\text{Si}} = 0.2$  kcal/mol, and  $\epsilon_{\text{O}} = 0.075$  kcal/mol); P4, the second set of reduced charges on Si and O and the new set of Lennard-Jones parameters ( $Q_{\text{Si}} = 0.70$ ,  $Q_{\text{O}} = -0.35$ ,  $\epsilon_{\text{Si}} = 0.2$  kcal/mol, and  $\epsilon_{\text{O}} = 0.075$  kcal/mol); and P5, no charges on Si and O and the new set of Lennard-Jones parameters ( $Q_{\text{Si}} = 0.0$ ,  $Q_{\text{O}} = 0.0$ ,  $\epsilon_{\text{Si}} = 0.2$  kcal/mol, and  $\epsilon_{\text{O}} = 0.075$  kcal/mol), which corresponds to mechanical embedding of the QM region. Reference to Table 1 shows that the charges on Si and O used here are significantly smaller than those previously reported.

## QM/MM VALIDATION

Figures 3–5 show the difference between the energy (adsorption energy or activation energy) determined by QM/MM and full QM for each member of the three test sets. The difference between the adsorption or activation energies determined from QM/MM and full QM calculations is sensitive in general to the choice of charges placed on Si and O and to the parameters of the Lennard-Jones potential. However, the sensitivity to the choices of charges and Lennard-Jones parameters depends on the test set examined. Figure 3 reveals that the heats of adsorption of  $\text{C}_1$ – $\text{C}_4$  alkanes are insensitive to the choice of the charges placed on Si and O but quite sensitive to the choice of Lennard-Jones parameters. When the values of these parameters found in the present study are used, the rms error between QM/MM and full QM is 0.3 kcal/mol for parameter set P5 (i.e., mechanical embedding) and is 0.4 kcal/mol for parameter set P3 ( $Q_{\text{Si}} = 0.8$  and  $Q_{\text{O}} = -0.4$ ).

By contrast for the second test set (shown in Figure 4), in which electrostatic adsorbate–zeolite interactions are significant, the difference in the adsorption energies determined from QM/MM and full QM calculation is sensitive to both the charges placed on the Si and O atoms of the zeolite lattice and the corresponding Lennard-Jones parameters. The smallest difference is obtained using parameter set P4; however, using parameter set P3 yields only slightly larger errors. It is also apparent that exclusion of electrostatic interactions (P5) leads to large

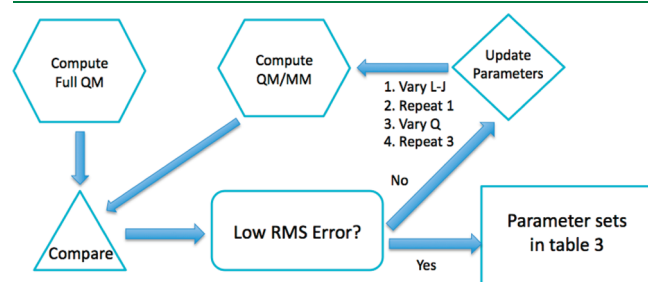
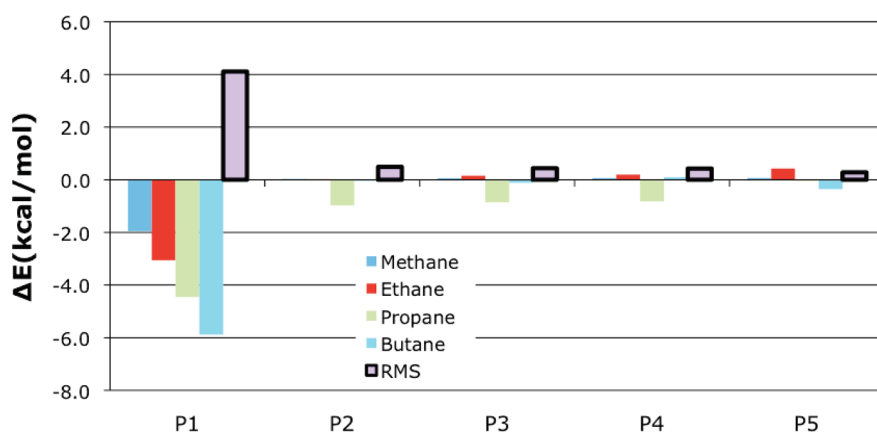


Figure 2. Schematic for generating Lennard-Jones and charge parameters.

Table 3. Charge and Lennard-Jones Parameters for O and Si Used in This Work<sup>a</sup>

parameter set	$Q_{\text{Si}}$	$Q_{\text{O}}$	$\epsilon_{\text{Si}}$ (kcal/mol)	$R_{\text{Si}}$ (Å)	$\epsilon_{\text{O}}$ (kcal/mol)	$R_{\text{O}}$ (Å)	$\Delta E_{\text{rms}}/6\text{-}31+\text{G}^{**}$ (kcal/mol)
P1	1.08	−0.54	0.6	2.2	0.1521	1.77	6.2
P2	1.08	−0.54	0.2	2.2	0.075	1.77	3.7
P3	0.8	−0.4	0.2	2.2	0.075	1.77	1.4
P4	0.7	−0.35	0.2	2.2	0.075	1.77	1.5
P5	0.0	0.0	0.2	2.2	0.075	1.77	8.1

<sup>a</sup> Adsorbate Lennard-Jones parameters are from the CHARMM force field.<sup>40</sup>



**Figure 3.** Energy differences between QM/MM and QM results (6-31+G\*\* basis) for alkanes adsorbed in all-silica T23 MFI. Alkane absorption is sensitive to Lennard-Jones parameters but insensitive to MM charges.

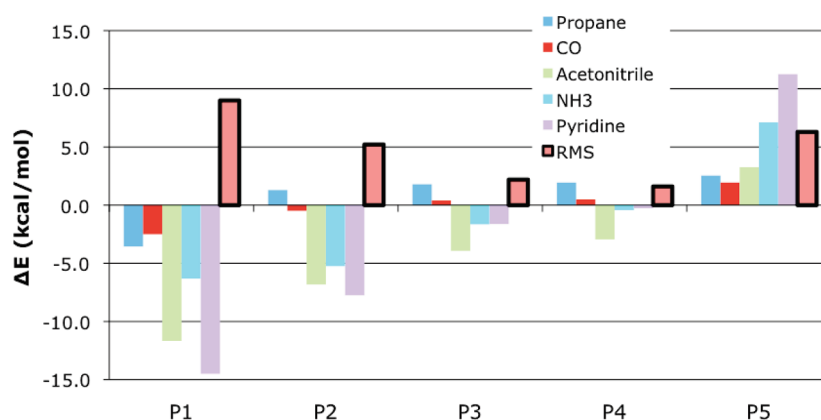


**Figure 4.** Energetic differences between QM/MM and QM results (6-31+G\*\* basis) for molecules adsorbed in T44 H-MFI. These adsorbed molecules are sensitive to both Lennard-Jones parameters and MM charges.

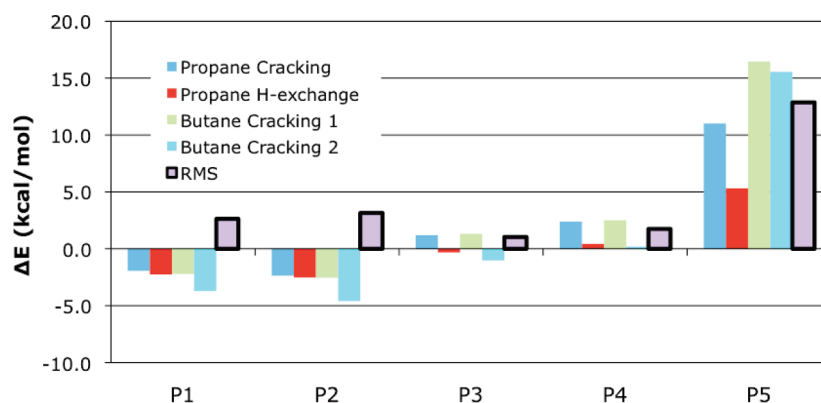


**Figure 5.** Energetic differences between QM/MM and QM results (6-31+G\*\* basis) for alkane activation in T23 H-MFI. Transition states are most sensitive to MM charge parameters, and mechanical embedding (P5) fails to reproduce QM results.

differences in the energies calculated from QM/MM and full QM. An even stronger effect of the charges placed on Si and O is evident for the calculation of activation energies for reactions involving propane and butane. In this case, the best agreement between QM/MM and full QM calculations is obtained using parameter set P3. When all three test sets are examined together, Figure 6 demonstrates that the

smallest rms difference in energies between the two computational strategies is obtained using parameter set P4.

QM/MM calculations carried out with the new charge and Lennard-Jones parameters also reproduced geometries obtained from full QM calculations. When single-point full QM energies were determined using fully converged QM/MM geometries,

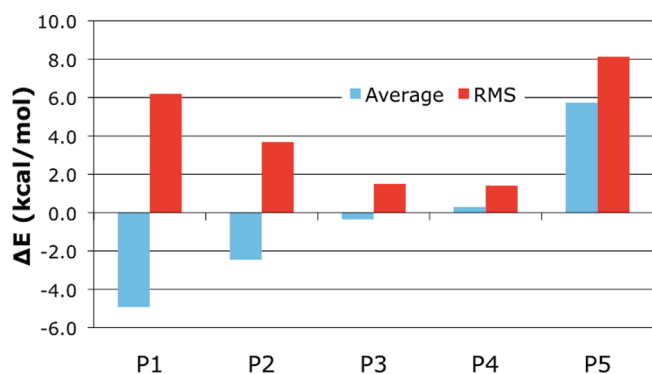


**Figure 6.** Energetic differences between QM/MM and QM results (6-31+G\*\* basis) averaged over the entire test set. The largest errors occur when mechanical embedding (zero charge in MM region, P5) is used and when charge and Lennard-Jones parameters are taken directly from an MM force field (P1).

**Table 4.** Difference in Energy from QM Single Points at QM/MM Optimized Geometries Compared to QM Optimized Geometries

		P3		P4	
		6-31G*	6-31+G**	6-31G*	6-31+G**
T23 MFI (all silica)	methane	0.0	0.0	0.0	0.0
	ethane	-0.5	-0.5	-0.5	-0.5
	propane	-0.3	-0.3	-0.3	-0.3
	butane	-0.2	-0.2	-0.1	-0.1
T44	propane	0.0	1.1	0.0	1.1
H-MFI	CO	0.0	0.4	0.0	0.2
	acetonitrile	1.7	0.6	1.7	0.6
	NH <sub>3</sub>	-0.7	0.3	-0.7	0.2
	pyridine	0.0	0.5	0.0	0.5
T23	propane cracking	-1.9	-0.6	-2.0	-0.7
H-MFI	propane H exchange	-2.5	-1.0	-2.4	-1.0
	butane cracking 1	1.3	0.5	1.2	0.4
	butane cracking 2	0.9	0.3	0.9	0.3
overall	average	-0.2	0.1	-0.2	0.1
	rms	1.0	0.6	1.1	0.6

the rms difference between QM energies at the full converged QM geometry and QM at the QM/MM geometry was less than 1 kcal/mol (see Table 4).

**Parameter Transferability.** To determine the transferability of the selected parameters, two additional tests were done. First, the entire test set was repeated with B3LYP and the 6-31G\* basis (see Table 2). To ensure a reasonable comparison, Lennard-Jones energies were removed from the QM/MM results because, as discussed earlier, the B3LYP functional does not account for dispersive interactions. Across the entire test set, QM/MM reproduces B3LYP energies with an rms difference of 1.8 kcal/mol with parameter set P4 and an rms difference of 2.2 kcal/mol with parameter set P3. In comparison, QM/MM with  $\omega$ B97X-D reproduces the QM energies with a 1.5 kcal/mol rms error, indicating that these parameters are likely transferable to other density functionals.

To test the transferability of the charges and Lennard-Jones parameters found to be best-suited for MFI, calculations were

**Table 5.** Single Point Energy Times from QM and QM/MM for Propane Adsorption

	time/SCF cycle		QM/MM speedup
	QM	QM/MM	
T5	9.2	N/A	1×
T23	769.2	14.6	53×
T44	9212.0	13.4	687×
in seconds			

carried out for the adsorption of CO, pyridine, and NH<sub>3</sub> at Brønsted acid sites in FAU. For these calculations, the framework of FAU was represented by a T52 cluster. For DFT calculations carried out at the  $\omega$ B97X-D/6-31G\* level, the rms errors in absorption energies obtained from QM and QM/MM were 2.0 kcal/mol for parameter set P4 and 3.7 kcal/mol for parameter set P3. Therefore, the charge and Lennard-Jones parameters that give accurate results for MFI are transferable to FAU and, by extension, to other zeolites.

As demonstrated by the current study, QM/MM calculations of adsorption and reaction occurring in cluster representations of zeolites can achieve accuracies rivaling those obtained from full QM calculations for clusters of the same size as that used for the QM/MM calculations. The significant difference, though, is that QM calculations in the QM/MM approach are done for only a T5 cluster electrostatically embedded in the remainder of the model cluster. This difference enables substantially faster computational times than can be achieved using a full QM approach. To demonstrate this point, Table 5 lists the times required for single point calculations of the energy for propane adsorption in MFI determined by QM and QM/MM as a function of the cluster size. It is evident that for a T23 cluster, QM/MM is over 50 times faster than QM, and for a T44 cluster, QM/MM is over 600 times faster than QM. This means that the QM/MM approach can be used to carry out calculations of adsorption and reaction processes using a very large overall cluster, which may contain multiple active sites.

## ■ ALKANE ACTIVATION IN LARGE ZEOLITE LATTICE

To demonstrate the lattice size approachable by QM/MM, parameter set P4 was used to investigate the cracking in MFI of *n*-alkanes<sup>42–47</sup> containing up to 18 carbon atoms. A cluster of about 1000 atoms (T356) was required to represent the straight channel of MFI so as to capture the effects of dispersive interactions for alkanes containing up to 18 carbon atoms (see Figure 7). The MFI zeolite includes a single acid site at the T12 position. The reacting molecules and a T5 active site are placed in the QM region of QM/MM. If a smaller cluster had been used, a part of the largest alkanes in the series would have spilled out of the cluster, and a similar problem would have arisen if we had tried to use a small repeated cell for periodic boundary calculations. Therefore, neither QM cluster simulations nor periodic simulations can handle the size of the cluster required to study linear alkanes with 18 carbon atoms. With  $\sim N^3$  scaling for DFT, such a large cluster would require approximately 5000 times the computational time required for a T23 cluster and hence would be prohibitive.

This setup is designed to demonstrate the ability of QM/MM to describe chemistries that require a large model zeolite, but we do not suggest that the absorption and cracking of C12 and C18 alkanes in the zeolite straight channel specifically represent the physical process in MFI. Instead, if C<sub>12</sub>H<sub>26</sub> or C<sub>18</sub>H<sub>38</sub> were to

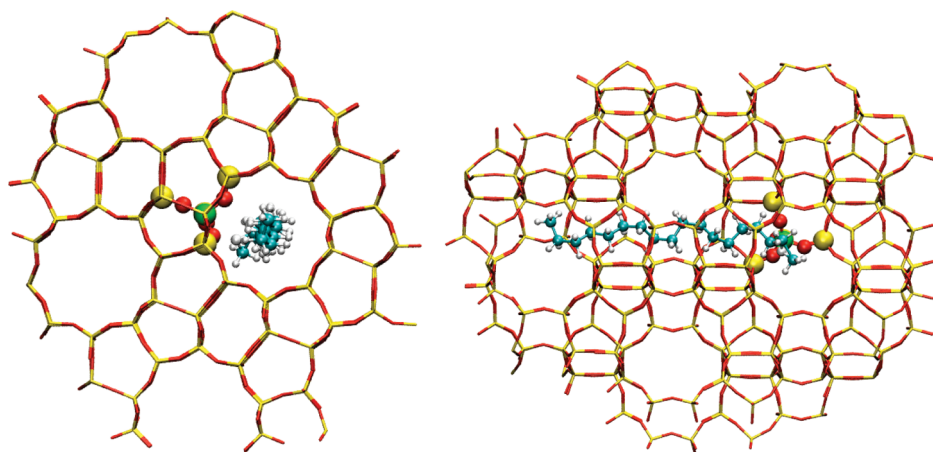


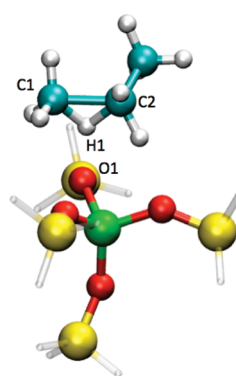
**Figure 7.** T356 MFI zeolite used for investigating the cracking of long alkanes. C18 is shown in the straight channel. The T5 QM region centered on the Al site is highlighted (view down straight channel on left, side view on right).

**Table 6.** Intrinsic Activation Barriers ( $\Delta H_{773K}^\ddagger$ ) for Terminal Carbon Cracking of  $C_3$ – $C_8$  Alkanes Determined via QM/MM  $\omega$ B97X-D/6-31G\* Using a T356 Representation of the Straight Channel in MFI with the Acid Site Located at the T12 Position

	Intrinsic Cracking Barrier, $\Delta H_{773K}^\ddagger$ (kcal/mol)	
	T356	exp.
$C_3H_8$	40.4	46.1, <sup>61</sup> 47.3 <sup>60</sup>
$C_6H_{14}$	36.3	47.1 <sup>60</sup>
$C_{12}H_{22}$	35.1	N/A
$C_{18}H_{38}$	37.3	N/A

diffuse into MFI, cracking may begin prior to complete absorption. For this reason, we emphasize that the following results are specifically based on the assumption that the long chain alkanes diffuse to an absorption site in a zeolite straight channel without being cracked prior to absorption.

Table 6 lists the intrinsic activation enthalpy for  $C_3$  through  $C_{18}$  for terminal C–C bond cracking determined at the  $\omega$ B97X-D/6-31G\* level of theory. The intrinsic activation enthalpy for propane cracking (i.e., the energy difference between the transition state and propane absorbed at the acid site) is 40.4 kcal/mol. This value is 4.8 kcal/mol lower than that determined at the same level of theory using a T23 cluster. The lower barrier height determined for the larger cluster is due to the additional electrostatic stabilization of the separated charges in cracking TSs and indicates the significance of long-range interactions that are missed by small cluster models. For cracking at an acid site positioned at T12, QM/MM with  $\omega$ B97X-D/6-31G\* underestimates the experimentally determined intrinsic barrier heights for cracking of terminal C–C bonds in propane and hexane by 7–10 kcal/mol. To determine how sensitive the cracking barrier was to the acid site position, the cracking barriers for propane and hexane were determined with the acid site positioned at T3. With this acid site, the intrinsic activation barriers rose by 3.2 and 5.8 kcal/mol, for propane and hexane, respectively, indicating significant variance due to acid site position. These barriers therefore come within about 4 kcal/mol of the experimental



Comparison of atomic distances calculated by QM/MM using T23 and T356 cluster representations of MFI

$C_3H_8$	Distance in Å	
	T23 Cluster	T356 Cluster
C1–C2	1.808	1.755
C1–H1	1.244	1.303
C2–H1	1.314	1.333
O1–H1	1.873	1.709

Effect of alkane length on bond distances determined by QM/MM using a T356 representation of MFI

	Distance in Å			
	$C_3H_8$	$C_6H_{14}$	$C_{12}H_{26}$	$C_{18}H_{38}$
C1–C2	1.755	1.730	1.780	1.788
C1–H1	1.303	1.327	1.293	1.287
C2–H1	1.333	1.318	1.268	1.269
O1–H1	1.709	1.698	1.860	1.858

**Figure 8.** Geometric distances for cracking reactions in T23 MFI cluster compared to the large (T356) MFI cluster. Both zeolites contain the acid site at the T12 position. Only the T5 QM region is shown, and geometries are qualitatively similar for cracking of the longer alkanes.

values. This is by no means a complete sampling of the variety of acid sites in MFI, so a complete theoretical study of alkane activation will require systematic investigation of the effect of the acid site to provide a quantitative comparison to experimental results.

The geometries for cracking reactions are somewhat dependent on the size of the zeolite cluster model and the alkane length. Figure 8 shows a comparison of cracking geometries from T23 and the large zeolite for reactions with the T12 acid site. These geometries are compared via examination of the distances between the acid active site oxygen, the proton, and the two carbon atoms undergoing cracking. While the smaller T23 zeolite qualitatively reproduces the larger zeolite's cracking geometries for propane, the O–H distance at the TS is longer by about 0.16 Å. This indicates that the missing long-range electrostatics cause an approximate description of the TS geometry. This suggests that previous simulations with smaller clusters (i.e., T23, T44) can yield useful information about zeolite reactivity but are still incomplete descriptions of chemistries like alkane cracking. Furthermore, smaller model clusters will inevitably leave out the



shape selectivity inherent to the zeolite structure and cannot model any reactivity that depends on extended zeolite structure.

There is a small but significant difference in the alkane cracking geometries when comparing the shorter alkanes to the longer alkanes. Specifically, the O–H distance for the shorter alkanes is about 0.15 Å shorter than in the longer alkanes. This difference can be attributed to the steric constraints of adsorbing and cracking C12 and C18 in the straight channel. The longer alkanes do not have the same degree of steric flexibility as C3 and C6, forcing the proton to be slightly further away from the acid site at the cracking geometry. Because the potential energy surface in zeolites is relatively flat due to the long-range electrostatics and dispersion of the lattice, multiple minima corresponding to the same TS may be present. To determine whether this was true, we reoptimized the TSs for C12 and C18 starting from geometries with quantitatively similar bond lengths as C3. However, the TS searches resulted in the same geometries as determined previously, indicating that the shorter and longer alkanes can be differentiated on the basis of the steric properties of their absorption in the large zeolite lattice.

## CONCLUSIONS

Hybrid QM/MM simulations that provide similar accuracy to full QM simulations have been achieved over a diverse test set of zeolite interactions and reactions. Although QM/MM has been known to be a computationally efficient method (about 50× faster than QM for a T23 zeolite compared to QM/MM with a T5 QM region, 700× faster for T44), its accuracy is shown to be highly dependent on the quality of the MM parameters. As Table 1 shows, there is no agreement in the literature on the appropriate atomic partial charges, and up to this point, no systematic testing has been done to validate charge parameters for QM/MM. In QM/MM simulations, utilizing charge parameters designed for MM is inappropriate without careful validation.

Parameters specifically selected for QM/MM in zeolites are provided herein (see Table 5) and are useful for electrostatically embedded QM/MM implementations. The Lennard-Jones parameters are chosen for compatibility with CHARMM adsorbate parameters. The selected parameters provide an accuracy of about 1.5 kcal/mol and reproduce QM structures to within 1.0 kcal/mol when a T5 cluster is used for the QM region. These errors are quite low and demonstrate the applicability of static point charges and single hydrogen link atoms for QM/MM simulations. This accuracy, however, could still be improved by accounting for polarization in the MM region or improved link atom representations. Because the parameters are applicable to  $\omega$ B97X-D and B3LYP functionals as well as MFI and FAU zeolites, we anticipate that they will be generally useful for QM/MM zeolite simulations.

The accuracy of zeolite simulations depends strongly on the quality of the density functional as well as the MM parameters. The results of this study suggest that density functionals that capture dispersion interactions should be used whenever possible, and dispersion corrections should also be applied between MM–QM atom pairs. This is exemplified in Table 2, where B3LYP poorly reproduces experimental heats of absorption and apparent activation energies. Furthermore, examination of Table 3 and Figure 6 shows that neglect of electrostatics (i.e.,  $Q_{\text{Si}} = Q_{\text{O}} = 0$  mechanical embedding) outside of the T5 cluster produces results that are far from convergence. QM/MM simulations that reproduce the results of density functionals such as  $\omega$ B97X-D provide an efficient avenue for examining complex shape-selective reactivity in zeolites.

## AUTHOR INFORMATION

### Corresponding Author

\*E-mail: mhg@cchem.berkeley.edu.

## REFERENCES

- (1) Corma, A. *Chem. Rev.* **1995**, 95, 559–614.
- (2) Smit, B.; Maesen, T. L. M. *Chem. Rev.* **2008**, 108, 4125–4184.
- (3) Vermeiren, W.; Gilson, J.-P. *Top. Catal.* **2009**, 52, 1131–1161.
- (4) Yu, J.; Xu, R. *Acc. Chem. Res.* **2010**, 43 (9), 1195–1204.
- (5) Traa, Y.; Burger, B.; Weitkamp, J. *Microporous Mesoporous Mater.* **1999**, 30, 3–41.
- (6) Marcilly, C. R. *Top. Catal.* **2000**, 13, 357–366.
- (7) Ribeiro, M.F., J. M. J. *Mol. Cat. A* **1995**, 96, 245–270.
- (8) Rigutto, M. S. In *Zeolites and Related Materials: Trends, Targets and Challenges*; Gedeon, A., Massania, P., Babonneau, F., Eds; Elsevier: Amsterdam, 2008; Vol 174, pp 43–52.
- (9) Sastre, G.; Corma, A. *J. Mol. Cat. A* **2009**, 305, 3–7.
- (10) Ribeiro, F. R.; Alvarez, F.; Henriques, C.; Lemos, F.; Lopes, J. M.; Ribeiro, M. F. *J. Mol. Cat. A* **1995**, 96, 245–270.
- (11) Broadbelt, L. J.; Snurr, R. Q. *App. Catal. A* **2000**, 200, 23–46.
- (12) Tafipolsky, M.; Amirjalayer, S.; Schmid, R. *Microporous Mesoporous Mater.* **2010**, 129, 304–318.
- (13) (a) Hohenberg, P.; Kohn, W. *Phys. Rev.* **1964**, 136, B864. (b) Kohn, W.; Sham, L. J. *Phys. Rev.* **1965**, 140, A1133.
- (14) (a) Becke, A. D. *Phys. Rev. A* **1988**, 38, 3098–3100. (b) Lee, C. T.; Yang, W. T.; Parr, R. G. *Phys. Rev. B* **1988**, 37, 785–789.
- (15) Zhao, Y.; Truhlar, D. G. *J. Phys. Chem. C* **2008**, 112 (17), 6860–6868.
- (16) Zhao, Y.; Truhlar, D. G. *Org. Lett.* **2006**, 8 (25), 5753–5755.
- (17) Zhao, Y.; Truhlar, D. G. *Theor. Chem. Acc.* **2008**, 120, 215.
- (18) (a) Chai, J.-D.; Head-Gordon, M. *Phys. Chem. Chem. Phys.* **2008**, 10, 6615–6620. (b) Chai, J.-D.; Head-Gordon, M. *J. Chem. Phys.* **2008**, 128, 084106.
- (19) (a) Blaszkowski, S. R.; Nascimento, M. A. C.; van Santen, R. A. *J. Phys. Chem.* **1996**, 100 (9), 3463–3472. (b) Boronat, M.; Viruela, P.; Corma, A. *J. Phys. Chem. A* **1998**, 102, 982–989.
- (20) Hansen, N.; Kerber, T.; Sauer, J.; Bell, A. T.; Keil, F. J. *J. Am. Chem. Soc.* **2010**, 132, 11525–11538.
- (21) Tuma, C.; Kerber, T.; Sauer, J. *Angew. Chem., Int. Ed.* **2010**, 49, 4678–4680.
- (22) Lin, H.; Truhlar, D. G. *Theor. Chem. Acc.* **2007**, 117, 185–199.
- (23) Bakowies, D.; Thiel, W. *J. Phys. Chem.* **1996**, 100, 10580–10594.
- (24) de Vries, A. H.; Sherwood, P.; Collins, S. J.; Rigby, A. M.; Rigutto, M.; Kramer, G. J. *J. Phys. Chem. B* **1999**, 103, 6133–6141.
- (25) Clark, L. A.; Sierka, M.; Sauer, J. *J. Am. Chem. Soc.* **2004**, 126, 936–947.
- (26) Lomratsiri, J.; Probst, M.; Limtrakul, J. *J. Mol. Graphics Model.* **2006**, 25, 219–225.
- (27) Shor, A. M.; Ivanova Shor, E. A.; Laletina, S.; Naslusev, V. A.; Vayssilov, G. N.; Rosch, N. *Chem. Phys.* **2009**, 363, 33–41.
- (28) Sierka, M.; Sauer, J. *Faraday Disc.* **1997**, 106, 41–62.
- (29) Sauer, J.; Sierka, M. *J. Comput. Chem.* **2000**, 21 (16), 1470–1493.
- (30) Svensson, M.; Humbel, S.; Froese, R. D. J.; Matsubara, T.; Sieber, S.; Morokuma, K. *J. Phys. Chem.* **1996**, 100 (50), 19357–19363.
- (31) Olson, D. H.; Koktailo, G. T.; Lawton, S. L.; Meier, W. M. *J. Phys. Chem. B* **1981**, 85, 2238–2243.
- (32) Olson, D. H. *Zeolites* **1995**, 15, 439–443.
- (33) Olson, D. H. *J. Phys. Chem. B* **2000**, 104, 4844–4848.
- (34) Mentzen, B. F.; Sacerdoteperonnet, M. *Mater. Res. Bull.* **1994**, 29, 1341–1348.
- (35) Shao, Y.; *Phys. Chem. Chem. Phys.* **2006**, 8, 3172–3191.
- (36) Woodcock, H. L.; Hodosek, M.; Gilbert, A. T. B.; Gill, P. M. W.; Schaefer, H. F.; Brooks, B. R. *J. Comput. Chem.* **2007**, 28 (9), 1485–1502.



- (37) Field, M. J.; Bash, P. A.; Karplus, M. *J. Comput. Chem.* **1990**, *11*, 700.
- (38) Shao, Y.; Kong, J. *J. Phys. Chem. A* **2007**, *111*, 3661.
- (39) Ferre, N.; Assfeld, X. *THEOCHEM* **2003**, 632, 83–90.
- (40) (a) Foloppe, N.; Mackerell, A. D. *J. Comput. Chem.* **2000**, *21* (2), 86–104. (b) Yin, D.; Mackerell, A. D. *J. Comput. Chem.* **1998**, *19* (3), 334–348. (c) Vanommeslaeghe, K.; Hatcher, E.; Acharya, C.; Kundu, S.; Zhong, S.; Shim, J.; Darian, E.; Guvench, O.; Lopes, P.; Vorobyov, I.; Mackerell, A. D. *J. Comput. Chem.* **2009**, *31* (4), 671.
- (41) Lopes, P. E. M.; Murashov, V.; Tazi, M.; Demchuk, E.; Mackerell, A. D. *J. Phys. Chem. B* **2006**, *110*, 2782–2792.
- (42) Swisher, J. A.; Hansen, N.; Maesen, T.; Keil, F. J.; Smit, B.; Bell, A. T. *J. Phys. Chem. C* **2010**, *114*, 10229–10239.
- (43) Kotrel, S.; Knozinger, H.; Gates, B. C. *Microporous Mesoporous Mater.* **2000**, 35–36, 11–20.
- (44) Haag, W. O. *Stud. Surf. Sci. Catal.* **1994**, *84*, 1375.
- (45) Kotrel, S.; Rosynek, M. P.; Lunsford, J. H. *J. Phys. Chem. B* **1999**, *103*, 818–824.
- (46) Katada, N.; Suzuki, K.; Noda, T.; Miyatani, W.; Taniguchi, F.; Niwa, M. *Appl. Catal. A: Gen.* **2010**, *373*, 208–213.
- (47) Babitz, S. M.; Williams, B. A.; Miller, J. T.; Snurr, R. Q.; Haag, W. O.; Kung, H. H. *Appl. Catal. A: Gen.* **1999**, *179*, 71–86.
- (48) Pantu, P.; Boekfa, B.; Limtrakul, J. *J. Mol. Cat. A* **2007**, *277*, 171–179. (b) Kasuriya, S.; Namuangruk, S.; Treesukol, P.; Tirtowidjojo, M.; Limtrakul, J. *J. Catal.* **2003**, *219*, 320–328. (c) Sung, C.-Y.; Broadbelt, L. J.; Snurr, R. Q. *J. Phys. Chem. C* **2009**, *113*, 15643–15651.
- (49) Nasluzov, V. A.; Ivanova, E. A.; Shor, A. M.; Vayssilov, G. N.; Birkenheuer, U.; Rosch, N. *J. Phys. Chem. B* **2003**, *107*, 2228–2241.
- (50) Shor, A. M.; Ivanova Shor, E. A.; Laletina, S.; Nasluzov, V. A.; Vayssilov, G. N.; Rosch, N. *Chem. Phys.* **2009**, *363*, 33–41.
- (51) Sherwood, P.; de Vries, A. H.; Collins, S. J.; Greatbanks, S. P.; Burton, N. A.; Vincent, M. A.; Hillier, I. H. *Faraday Discuss* **1997**, *106*, 79–92.
- (52) Injan, N.; Pannorad, N.; Probst, M.; Limtrakul, J. *Int. J. Quantum Chem.* **2005**, *105*, 898–905.
- (53) Stefanovich, E. V.; Truong, T. N. *J. Phys. Chem. B* **1998**, *102*, 3018–3022.
- (54) Sun, M. S.; Shah, D. B.; Xu, H. H.; Talu, O. *J. Phys. Chem. B* **1998**, *102*, 1466–1473.
- (55) Eder, F.; Stockenhuber, M.; Lercher, J. A. *J. Phys. Chem. B* **1997**, *101*, 5414–5419.
- (56) Savitz, S.; Myers, A. L.; Gorte, R. J. *J. Phys. Chem. B* **1999**, *103*, 3687–3690.
- (57) Szanyi, J.; Paffett, M. T. *Microporous Mater.* **1996**, *7*, 201–218.
- (58) Lee, C.-C.; Gorte, R. J.; Farneth, W. E. *J. Phys. Chem. B* **1997**, *101*, 3811–3817.
- (59) Parrillo, D. J.; Gorte, R. J. *Appl. Catal. A: Gen.* **1994**, *110*, 67–74.
- (60) Narbeshuber, T. F.; Vinek, H.; Lercher, J. A. *J. Catal.* **1995**, *157*, 388–395.
- (61) Xu, B.; Sievers, C.; Hong, S. B.; Prins, R.; van Bokhoven, J. A. *J. Catal.* **2006**, *244*, 163–168.